# Stacked Geodesic Lenses for Radar Applications in the W-Band

Germán León*, Omar Orgeira†, Nelson J. G. Fonseca‡, Oscar Quevedo-Teruel†
*Dept. of Electrical Engineering, Universidad de Oviedo, Gijón, Spain, gleon@uniovi.es
†Divison of Electromagnetic Engineering, KTH Royal Institute of Technology, Stockholm, Sweden
‡Antenna and Sub-Millimetre Waves Section, European Space Agency, Noordwijk, The Netherlands

***Abstract*—New radar architectures employ multiple transmitters and receivers to enhance their performance, combining wide and narrow beams to improve the spatial resolution. In this contribution, two antenna system configurations based on stacked geodesic lenses are compared. These lenses are fully-metallic parallel plate waveguides that present very low transmission losses in the millimetre-wave band. Narrow beams are generated by a 15-port Luneburg-Rinehart lens with a scanning span of $\pm 50^\circ$ and 23.4 dB gain at 77 GHz. For wide beams, two alternatives are proposed. One alternative is a 3-port defocused lens antenna with a scanning angle of $\pm 50^\circ$ and 14.5 dBi gain. The second proposal is a 12-port Luneburg-Rinehart lens fed with 1-to-4 power dividers forming a 3-port antenna with a scanning span of $\pm 45.5^\circ$ and 16.2 dBi gain.**

***Index Terms*—Radar, lens antennas, geodesic lenses, Luneburg lens, near and far fields analysis, multiple beam antennas.**

## I. Introduction

Radar architectures can enhance their spatial resolution and mitigate scintillations by combining an array of a reduced number of transmitters (Tx) and a receiver (Rx) chain. Several radar applications are starting to take advantage of these architectures. For example, multiple-input multiple-output SAR (MIMO-SAR) configurations were proposed in [1], [2]. In [3], 4-Tx and 1-Rx is used for imaging applications to develop a virtual MIMO-SAR system. Also, automotive radar [4] and imaging applications [5] can exploit the benefits of these radio-frequency chains.

These applications require a combination of narrow and wide beams. Luneburg lenses [6] are good candidates to generate several independent narrow beams and wide scan angle due to their rotational symmetry. A dielectric Luneburg lens is characterized by a gradient of permitivity such that an isotropic radiation is transformed into a planar wave [4], [7]. However, dielectric materials introduce significant losses at millimetre-wave frequencies. Therefore, a solution in which the propagation is in air is preferable.

Geodesic lenses (GLs) can be constructed using parallel plate waveguide technology where the fields are confined between two metallic plates, thus forming a fully-metallic system. Consequently, they allow a propagation in air without dielectric losses. GLs can mimic the behaviour of a Luneburg lens and therefore, generate directive beams [8]-[12], or produce defocusing lenses to generate wider beams [13], [14].

In this paper, we present two alternatives to generate broadbeams using GLs, in Section II. One possibility is to use a near-field (NF) focusing lens that generates a wide beam in the far-field (FF). The second alternative is to use a 1-to-4 power divider to feed a Luneburg lens, generating wider beams as an aggregation of adjacent directive beams. In section III, we use the stacked-lens concept [15], [16] to generate a double lens configuration that is capable of generating simultaneously high directive and broadbeams.

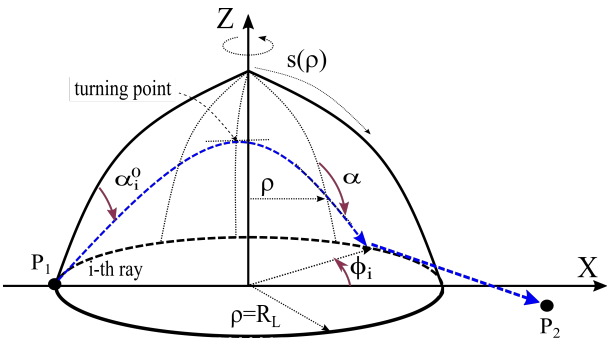


Fig. 1. Schematic representation of a ray propagation inside a near-field focusing geodesic lens.

## II. Broadbeam Geodesic Lens

A rotationally symmetric GL (Fig. 1) can be depicted by a radial coordinate $\rho$, an angular coordinate $\phi$ and the value of the function $s(\rho)$ that represents the length on the surface measured along the meridian from the axis of symmetry to the given point. In a GL, rays emerge from a point source $P_1[\rho_1 = R_L, \phi = \pi]$ and converge to a focal point $P_2[\rho_2 \geq R_L, \phi_2 = M\,\pi]$, where $M$ is a real number equal or greater than 1, such that $-M\,\pi$ corresponds to the total change of polar angle in radians swept by the ray during its propagation. For a fixed point $P_1$, the values of $\rho_2$ and $M$ determine the shape of the GL through the function $s(\rho)$. An analytical expression for $s(\rho)$ was derived in [17].

### A. Defocused Geodesic Lens

Defocused GLs focus the power to a point in the NF (see Fig. 2) resulting in a broadbeam in the FF. This capability is used in this work to design beams with different beamwidths. The authors developed a model to analyze the NF and the FF of a GL with rotational symmetry in [14], [18]. This algorithm combines ray tracing and Huygens' secondary-sources array

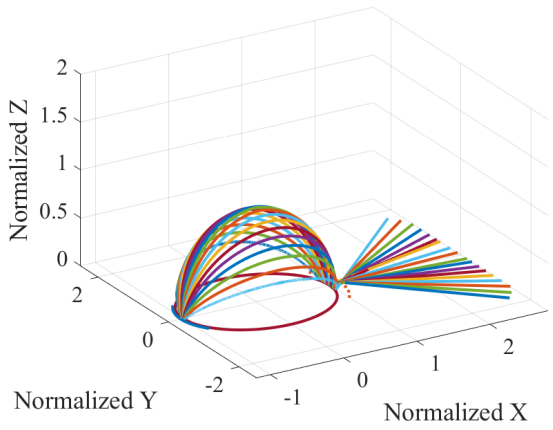


Fig. 2. Ray tracing of a defocused (near-field focusing) geodesic lens.

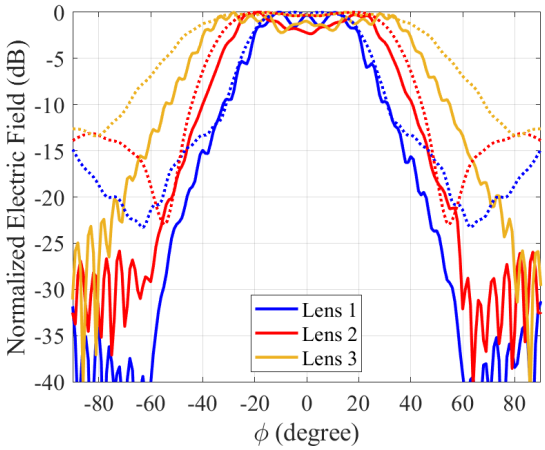


Fig. 3. H-plane radiation pattern comparison for the model proposed in [14], [18] (dotted lines) and HFSS (solid lines) for the geodesic lenses in Table I.

model to calculate the radiation pattern quickly and accurately. The algorithm needs few seconds in a regular laptop to calculate the FF of a GL antenna. This model has been applied to design defocused lenses with different 3-dB beamwidth in the FF. These designs have been compiled in Table I. All these examples are antennas at 77 GHz, with $R_L = 6\lambda = 23.4$ mm and $\rho_1 = 1.03\, R_L$. In Fig. 3, a comparison between the model and full-wave simulation results obtained with HFSS [19] is provided. The model allows to find lenses with good accuracy in the 3-dB beamwidth for *Lens 1* and *Lens 2*. However, when the beamwidth increases, the model reduces its agreement with the full-wave simulation. In this work, we aim for a lens with a 3-dB beamwidth of approximately $\pm 20°$. Therefore, *Lens 1* was selected for the final antenna design in Section III.A. The realized gain of these antennas is represented in Fig. 4. The maximum gain is reduced from 15.3 dBi for a lens with $\pm 20°$ beamwidth to 12.3 dBi for a lens covering $\pm 40°$.

TABLE I
GEODESIC LENS PARAMETERS FOR DIFFERENT BEAMWIDTHS.

| ID | $\rho_2/R_L$ | $M$ | Beamwidth (°) | Gain (dBi) |
|---|---|---|---|---|
| Lens 1 | 2.00 | 1.003 | ± 20 | 15.3 |
| Lens 2 | 1.50 | 1.010 | ± 30 | 13.5 |
| Lens 3 | 1.20 | 1.030 | ± 40 | 12.3 |

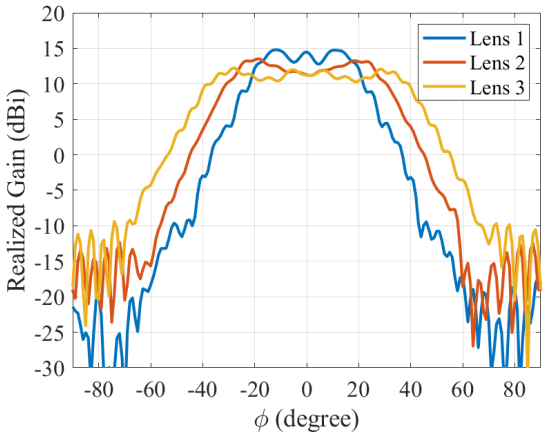


Fig. 4. H-Plane realized gain for the defocused geodesic lens antennas in Table I.

### B. Broadbeam Luneburg-Rinehart Lens

A Luneburg lens has the image focal point $P_2$ in the infinity $P_2[\rho_2 = \infty, \phi = 0]$. Therefore, this lens is capable of transforming an isotropic source point (cylindrical wave) into a planar wave and in turn, generates high directive beams in the FF. The ray tracing of the geodesic equivalent of a Luneburg lens is illustrated in Fig. 5. This lens is also known as Luneburg-Rinehart lens [8].

In order to produce a broader beam with a Luneburg lens, several ports can be fed simultaneously. For example, for a 12-port Luneburg lens, ports can be combined in three groups of 4 ports with the 1-to-4 power divider, as illustrated in Fig. 6, resulting in a modified 3-port Luneburg-Rinehart lens antenna.

The power divider was designed so that the four outputs are in phase across the whole band as shown in Fig. 7.(c). This is achieved equalizing the path lengths. This is of high importance as the phase of the feeding ports will determine the performance of our antenna. The design of the presented power divider has to account for the fact that the feeding ports are distributed over a circular curve. Indeed, the path length from the common port (1 in Fig. 6) toward the outer feeding ports (2 and 5 in Fig. 6) is geometrically longer than that toward the inner feeding ports (3 and 4 in Fig. 6). This problem was overcome by starting from a perpendicular point in the middle of the divider and then following completely symmetric paths for all the branches. Moreover, the losses introduced by this power divider are very low with a maximum of 0.12 dB at 78 GHz and a $|S_{11}|$ below -17 dB, as presented in Fig. 7.(b) and 7.(a).

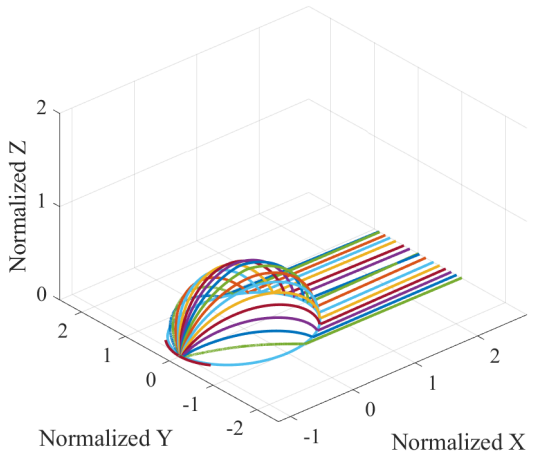


Fig. 5. Ray tracing for a Luneburg-Rinehart lens.

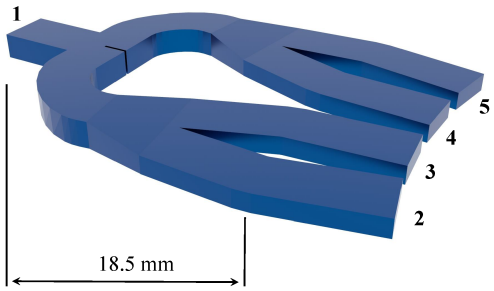


Fig. 6. 1-to-4 power divider to feed a 12-port Luneburg-Rinehart lens.

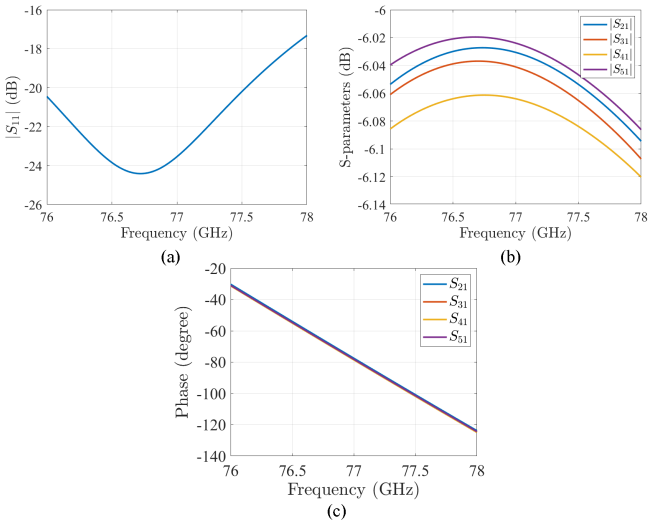


Fig. 7. S-parameters and output phase of the 1-to-4 power divider.

A Luneburg-Rinehart lens antenna fed with this power divider, as illustrated in the inset of Fig. 8, would produce a 3 dB beamwidth of $\pm 14.5\,^{\circ}$ and a maximum gain of 16.2 dBi with a ripple smaller than 1.5 dB.

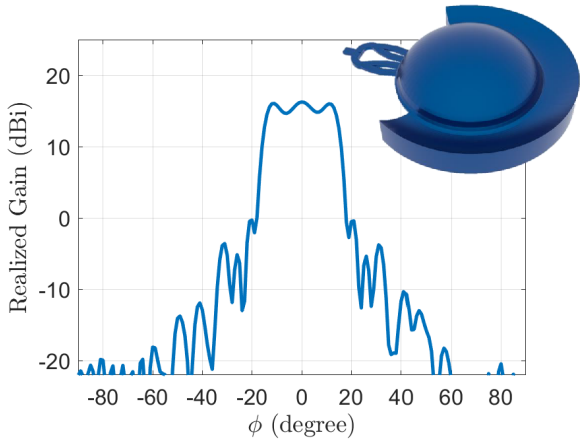


Fig. 8. H-plane radiation pattern generated by a Luneburg lens fed with a 1-to-4 power divider.

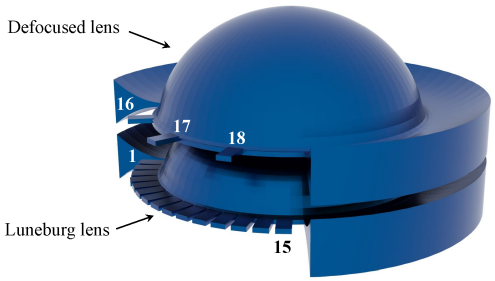


Fig. 9. Antenna system composed by two stacked GL: a 3-port defocused lens 1 (top) and a 15-port Luneburg-Rinehart lens (bottom).

## III. Double Lens Antenna Configuration

### A. *Defocused & Luneburg-Rinehart lens system*

An antenna system composed by a 3-port defocused lens and a 15-port Luneburg-Rinehart lens is illustrated in Fig. 9. The defocused lens has a greater height, so it should be placed on top for better integration. The separation between both lenses is 11 mm and the transmission coefficient between any ports in the top lens and any ports in the bottom lens is below -45 dB. Due to the rotational symmetry of the GLs, the shape of the beams does not change and the scan losses remain marginal.

This antenna system is able to cover an angular range of $\pm 50°$ with both antennas as shown in Fig. 10. The defocused antenna generates three wide beams whereas the Luneburg-Rinehart lens antenna generates 15 directive beams. The crossover point between two adjacent wide beams is below 2 dB and 6 dB, respectively. The E-plane radiation pattern mainly depends on the flare profile and it is not distorted by stacking the lenses as it can be seen in Fig. 11.

### B. *Two-Luneburg-Rinehart lens system*

Following the same procedure than in the previous subsection but utilising a double Luneburg-Rinehart lens configura-

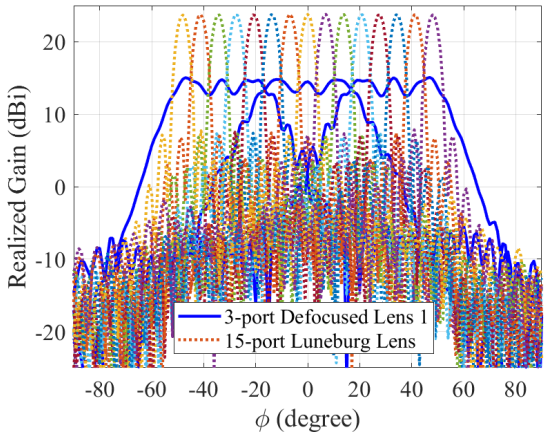


Fig. 10. Realized gain of the stacked 3-ports defocused GL (solid lines) and 15-ports Luneburg-Rinehart GL (dotted lines).

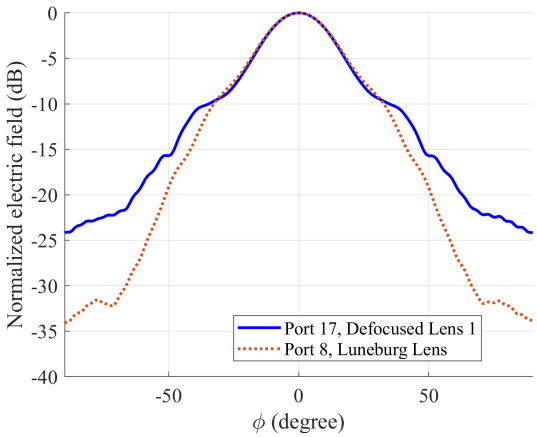


Fig. 11. Normalized E-plane radiation pattern of the stacked 3-ports defocused GL (port 17, solid lines) and 15-ports Luneburg-Rinehart GL (port 8, dotted lines).

tion (with and without combining the ports), we can mimic the behaviour. This configuration is shown in Fig. 12. Note that in this case the lenses are perfectly interchangeable due to the fact that they have same shape. We placed the 15-port Luneburg-Rinehart lens on top of the 3-port Luneburg-Rinehart lens with power dividers. The separation between the pair of antennas is again 11 mm. The mutual coupling between any ports of the two different antennas is below - 31 dB.

The behaviour of the 15-port Luneburg-Rinehart lens is the same than in the previous case. However, the 3-port Luneburg-Rinehart lens with power dividers has slightly less scan range across its field of view because of the abrupt decay of the lobes. With this configuration, we are able to scan over a $\pm 45.5°$ angle as shown in Fig. 13. Extending the range would be possible using instead 1-to-5 power dividers at the expense of a more complex design.

It appears that the two configurations lead to similar RF performance, with the solution combining a Luneburg lens

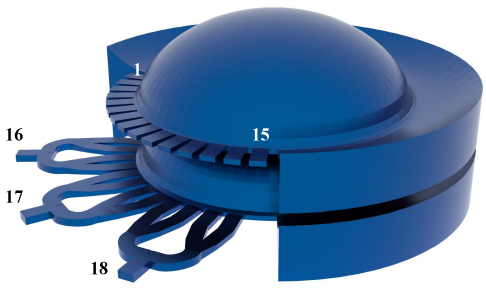


Fig. 12. Antenna system composed by two stacked GL: a 3-port Luneburg lens fed with three 1-to-4 power dividers (bottom) and a 15-port Luneburg lens (top).

and power dividers demonstrating slightly higher directivity and higher isolation between beams. The solution based on the defocused lens has slightly degraded performance, but is mechanically simpler, which could be advantageous with certain manufacturing techniques, such as casting.

Casting can give the best results in terms of tolerances and surface roughness, but the high cost of the mold makes it very expensive for a prototyping phase and only suitable for mass production. Consequently, other manufacturing technologies can be considered, such as CNC milling, which can achieve good tolerances. Nonetheless, the lenses have to be manufactured in several parts and then assembled together. This can lead to misalignments and, in turn, losses and a degradation of the performance of the antenna. Alternatively, 3D printing technology can be used in either its plastic metallized form or directly in metal. In the first option, typically the lens must be manufactured in two parts so the metallization can be properly applied. Furthermore, the antenna would be very sensitive to the metallization process since it has to ensure that the thickness and homogeneity of the coating are correct. However, fully-metallic 3D printing allows to take advantage of the main feature of the 3D printing technology, which is that the lenses can be manufactured in a single piece, avoiding misalignment issues. As a drawback, this technology still has to improve regarding surface roughness, but it has a strong potential.

The possibility of manufacturing this stacked antenna by means of any of the presented technologies shows the flexibility of the concept. The selected manufacturing technology will depend on the purpose of the fabrication, i.e. prototype, proof-of-concept, or mass production. In any case, good results can be expected from any of the techniques as long as the mechanical design of the antenna is properly developed for that technique.

## IV. Conclusion

In this paper we proposed two different alternatives of a stacked GL configuration to generate broad and narrow beams simultaneously. An algorithm previously developed by the authors was used to find geodesics curve that generate beams

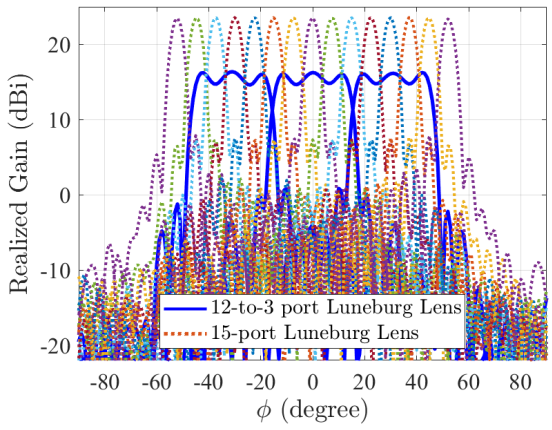


Fig. 13. Realized gain of the two Luneburg-Rinehart lens configuration.

with different 3-dB beamwidth. Therefore, an antenna system is proposed by combining a 3-ports GL antenna with wide beam as a transmitter for radar application meanwhile a 15-port geodesic Luneburg-Rinehart lens is used as a receiver to accurately determine the position of the target.

Furthermore, as an alternative, we also proposed a stack of two Luneburg-Rinehart lenses, one with 15 ports and another one with 12 ports that are reduced to 3 ports through the use of 1-to-4 power dividers. This alternative presents slightly less scanning range but better gain. Both proposals show the flexibility of these techniques to generate antennas of different beamwidths.

## ACKNOWLEDGMENT

This work has been supported in part by the Spanish Ministry of Science and Innovation and the Spanish Research Agency, under projects ARTEINE (TEC2017-86619-R), ENHANCE-5G (PID2020-114172RB-C21 / AEI / 10.13039/501100011033) and IDI/2021/000097 (Gobierno del Principado de Asturias). The work of O. Quevedo-Teruel was sponsored by the Office of Naval Research (ONR), under grant number N62909-20-1-2040. The views and conclusions contained herein are those of the authors only and should not be interpreted as representing those of ONR, the U.S. Navy or the U.S. Government.

## REFERENCES

[1] G. Krieger, "MIMO-SAR: Opportunities and pitfalls," *IEEE Trans. Geosci. Remote Sens.*, vol. 52, no. 5, pp. 2628–2645, 2014.

[2] J. Wang, X.-D. Liang, L.-Y. Chen, and Y.-L. Li, "First demonstration of airborne MIMO SAR system for multimodal operation," *IEEE Trans. Geosci. Remote Sens.*, pp. 1–13, 2021.

[3] A. Jouadé, S. Méric, O. Lafond, M. Himdi, and L. Ferro-Famil, "A passive compressive device associated with a Luneburg lens for multibeam radar at millimeter wave," *IEEE Antennas Wirel. Propag. Lett.*, vol. 17, no. 6, pp. 938–941, 2018.

[4] M. K. Saleem, H. Vettikaladi, M. A. S. Alkanhal, and M. Himdi, "Lens antenna for wide angle beam scanning at 79 GHz for automotive short range radar applications," *IEEE Trans. Antennas Propag.*, vol. 65, no. 4, pp. 2041–2046, 2017.

[5] S. Abid, C. Decroze, M. Mouhamadou, and T. Fromenteze, "Enhancing millimeter-wave computational interferometric imaging," *IEEE Access*, vol. 8, pp. 101416–101425, 2020.

[6] R. K. Luneburg, "Mathematical theory of optics," *Providence, Brown University Press*, 1944.

[7] R. M. Moreno, J. Ala-Laurinaho, and V. Viikari, "Plastic-filled dual-polarized lens antenna for beam-switching in the Ka-band," *IEEE Antennas Wirel. Propag. Lett.*, vol. 18, no. 12, pp. 2458–2462, 2019.

[8] R. Rinehart, "A solution of the problem of rapid scanning for radar antennae," *J. Appl. Phys.*, vol. 19, no. 9, pp. 860–862, Sep. 1948.

[9] Q. Liao, N. J. G. Fonseca, and O. Quevedo-Teruel, "Compact multibeam fully-metallic geodesic Luneburg lens antenna based on non-Euclidean transformation optics," *IEEE Trans. Antennas Propag.*, vol. 66, no. 12, pp. 7383–7388, 2018.

[10] N. J. G. Fonseca, Q. Liao, and O. Quevedo-Teruel, "Equivalent planar lens ray tracing model to design modulated geodesic lenses using non-Euclidean transformation optics," *IEEE Trans. Antennas Propag.*, vol. 68, no. 5, pp. 3410–3422, 2020.

[11] N. J. G. Fonseca, Q. Liao, and O. Quevedo-Teruel, "Compact parallel-plate waveguide half-Luneburg geodesic lens in the Ka-band," *IET Microw. Antennas Propag.*, vol. 15, no. 2, pp. 123–130, Feb. 2021.

[12] N. J. G. Fonseca, "The water drop lens: revisiting the past to shape the future," *EurAAP Reviews Electromag.*, vol. 1, no. 1, pp. 1–4, Sept. 2021.

[13] P.-Y. Feng, S.-W. Qu, and S. Yang, "Defocused cylindrical Luneburg lens antennas with phased array antenna feed," *IEEE Transactions on Antennas and Propagation*, vol. 67, no. 9, pp. 6008–6016, 2019.

[14] O. Orgeira, G. León, N. J. G. Fonseca, P. Mongelos, and O. Quevedo-Teruel, "Near-field focusing multibeam geodesic lens antenna for stable aggregate gain in far-field," *IEEE Trans. Antennas Propag.*, (early access).

[15] F. Doucet *et al.*, "Shaped continuous parallel plate delay lens with enhanced scanning performance," *IEEE Trans. Antennas Propag.*, vol. 67, no. 11, pp. 6695–6704, 2019.

[16] P. Castillo-Tapia, Q. Liao, N. J. G. Fonseca, and O. Quevedo-Teruel, "Modulated geodesic lens antenna array," in *2021 15th European Conference on Antennas and Propagation (EuCAP)*, pp. 1–4, 2021.

[17] M. Šarbort and T. Tyc, "Spherical media and geodesic lenses in geometrical optics," *J. Opt.*, vol. 14, no. 7, p. 075705, 2012.

[18] G. Leon, O. Orgeira, N. J. G. Fonseca, and O. Quevedo-Teruel, "Ray-tracing analysis of the near and far fields of focusing geodesic lens antennas," *14th European Conf. Antennas Propag. (EuCAP), Copenhagen, Denmark*, 2020.

[19] A. Corp., "Ansys® Electromagnetics Suite , release 2020 R1," Pittsburgh, PA. USA. 2018.